Polymer 51 (2010) 2629–2635

Contents lists available at ScienceDirect

Polymer

journal homepage: www.elsevier.com/locate/polymer

Preparation and properties of poly(ethylene glycol)-*block*-poly-(acrylic acid)-coated cobalt nanocrystals

Nemesio Martinez-Castro, Zhihan Zhou, Guojun Liu*

Department of Chemistry, Queen's University, 90 Bader Lane, Kingston, Ontario K7L 3N6, Canada

ARTICLE INFO

Article history:
Received 15 December 2009
Received in revised form
15 April 2010
Accepted 17 April 2010
Available online 24 April 2010

Keywords:
Co nanocrystals
Block copolymers
Magnetic materials

ABSTRACT

Reported in this paper are the preparation and properties of ε-Co nanocrystals coated by poly(ethylene glycol)-*block*-poly(acrylic acid) (PEG-*b*-PAA). These particles were prepared via the thermal decomposition of $Co_2(CO)_8$ at 185 °C in 1,2-dichlorobenzene, in the presence of the surfactant PEG-*b*-PAA and the co-surfactant trioctylphosphine oxide. At a given initial $Co_2(CO)_8$ concentration, the size of the particles increased with increasing $Co_2(CO)_8$-to-PEG-*b*-PAA molar ratio, and could be tuned between ~5 and ~20 nm. The size distribution of the particles narrowed as the $Co_2(CO)_8$ concentrations increased. The resultant particles were dispersible in a wide range of solvents, including chloroform, *N*,*N*-dimethylforamide, and water, which solubilized PEG. Magnetic measurements revealed that the particles possessed saturation magnetization close to that of bulk Co, suggesting high purity of the particles.

1. Introduction

Co nanocrystals may be used in immunoassays [1], in electromagnetic shielding [2], in electric devices [3], and for information storage [4,5]. Because of these potential applications, there have been many reports on their preparation and study [6,7]. Traditionally, Co nanoparticles are prepared from the high-temperature decomposition of a Co(0) precursor [8,9] or the high-temperature reduction [10,11] of a Co(II) precursor in the presence of a surfactant (e.g. oleic acid) and a co-surfactant (e.g. trioctyl phosphine oxide, or TOPO). The surfactants were used to regulate the growth and to render colloidal stability to the resultant Co nanoparticles. Aside from using small-molecule surfactants, random copolymers[12,13] and end-functionalized copolymers [14,15] have also been used as surfactants. There have been very few reports of the use of block copolymers as the surfactant [16,17]. We report in this paper the preparation of Co nanocrystals using poly(ethylene glycol)-*block*-poly(acrylic acid) (PEG-*b*-PAA) as the surfactant. We examine factors affecting the size and size distribution of the resultant Co nanocrystals.

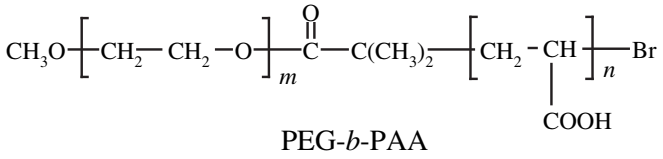

PEG-*b*-PAA

The Co nanocrystals described here were prepared by the rapid decomposition of $Co_2(CO)_8$ in anhydrous 1,2-dichlorobenzene at 185 °C using PEG-*b*-PAA and TOPO as the surfactant and co-surfactant, respectively. This method is similar to those used by Puntes et al. [6,9,18] and by Dinega et al. [19], except for the replacement of the small-molecule surfactants used in those procedures by our diblock surfactant, PEG-*b*-PAA. Co nanoparticles coated by PEG were targeted, because PEG is ion conductive. We speculated that these particles might be useful in polymer light-emitting electrochemical cells [20,21] or in batteries [22,23].

Aside from the high-temperature methods mentioned above for Co nanoparticle preparation, other methods have also been used to prepare polymer-coated Co nanoparticles. For example, Co nanoparticles have been prepared in the poly(4-vinyl pyridine) cores of spherical micelles of polystyrene-*block*-poly(4-vinyl pyridine) (PS-*b*-PVP) [24–28]. This preparation typically involved three steps, consisting of micelle preparation, loading of Co^{2+} into the micellar cores, and then Co^{2+} reduction. For cases when Co^{2+} was reduced at room temperature, several Co particles were often produced within each micelle core. Co nanoparticles have also been prepared in the tubular cores of ABC triblock copolymer nanotubes [29] and in the ionic domains of a Nafion® membrane [30]. The size distribution of these particles was wide. Besides Co nanoparticles, the block copolymer template approach has been used to prepare nanoparticles of other metals including Au, Pd, and Pt, as well as metal oxides and semiconductors [31–44]. Such templates can be the

* Corresponding author.
E-mail address: gliu@chem.queensu.ca (G. Liu).

0032-3861/$ – see front matter © 2010 Elsevier Ltd. All rights reserved.
doi:10.1016/j.polymer.2010.04.036

cores of block copolymer micelles formed in a block-selective solvent, or domains formed in a solid block copolymer.

2. Experimental section

2.1. Materials

The monomer *tert*-butyl acrylate (tBA, Aldrich, 99%) was stirred over CaH_2 for 12 h before purification by vacuum distillation. Copper (I) bromide (CuBr, 99.999%), *N,N,N,N,N*-pentamethyldiethylenetriamine (PMDETA, 99%), 2-bromoisobutyryl bromide (98%), trifluoroacetic acid (TFA, 98%), triethylamine (TEA, 99.5%), trioctyl phosphine oxide (TOPO, 90%), cobalt carbonyl $Co_2(CO)_8$ (90–95%), and diethyl ether (anhydrous, 99.7%) were all used as received from Aldrich. Toluene (Aldrich, 99.8%) was distilled over CaH_2 before use. Tetrahydrofuran (THF, 99.0%) and dichloromethane (99.5%) were purchased from Caledon and were used as received. Poly(ethyleneglycol monomethyl ether) (PEG-OH, $M_n = 5000$ g/mol, $M_w/M_n = 1.10$) was purchased from Scientific Polymer Products Inc., and vaccum-dried before use.

1,2-Dichlorobenzene (anhydrous, 99%, Aldrich), 200 mL, was washed with 30 mL of 98% H_2SO_4. It was then washed with deionized water six times, using 50 mL each time. After drying over $CaCl_2$ overnight, the supernatant was stirred with CaH_2 at 60 °C for 24 h before it was distilled under vacuum.

2.2. Synthesis of α-methoxy-ω-bromoisobutyrate poly (ethyleneglycol)

PEG-OH (5.0 g, 1.0 mmol) was dissolved in 300 mL of toluene in a three-neck round-bottom flask under magnetic stirring. TEA (0.28 mL, 2.0 mmol) was then added to this solution. This was followed by the dropwise addition at room temperature of 2-bromoisobutyryl bromide (0.25 mL, 2.0 mmol). After 48 h of stirring, the resultant suspension was filtered, and the filtrate was concentrated to 75 mL. Adding the filtrate into 600 mL of diethyl ether yielded α-methoxy-ω-bromoisobutyrate poly(ethyleneglycol) (PEG-Br) as a precipitate, which was then dried under vacuum.

2.3. PEG-b-PtBA

PEG-*b*-PtBA was synthesized by atom transfer radical polymerization (ATRP). A typical polymerization involved first charging a two-neck round-bottom flask with PEG-Br (1.0 g, 0.20 mmol), tBA (0.27 mL, 1.9 mmol), PMDETA (0.083 mL, 0.39 mmol), and 10 mL of distilled toluene. After degassing, CuBr (0.028 g, 0.20 mmol) was added under nitrogen flow. The flask was subjected to three freeze-thaw evacuation-and-nitrogen-filling cycles before it was immersed in an oil bath that was preheated to 80 °C. After tBA polymerization at 80 °C overnight, the resultant mixture was diluted with THF and passed through a neutral alumina column in order to remove the catalysts. After concentrating to 5 mL by rotary evaporation, the concentrate was added into 400 mL of diethyl ether in order to precipitate the polymer. The polymer was then dried under vacuum to yield 0.98 g of product.

2.4. PEO-b-PAA

A typical preparation involved stirring 0.98 g of PEG-*b*-PtBA with 3 mL of trifluoroacetic acid and 20 mL of methylene chloride for 3 h. The resultant mixture was added into 400 mL of diethyl ether in order to precipitate the product, PEO-*b*-PAA. The precipitate was then re-dissolved into 10 mL of dichloromethane and added into diethyl ether again. This procedure was repeated before the final precipitate was dried under vacuum at room temperature to yield 0.83 g of product.

2.5. Polymer characterization

^{1}H-NMR analyses were performed using a Bruker DRX-300 spectrometer, and spectra of PEG-*b*-PtBA and PEG-*b*-PAA were recorded in $CDCl_3$ and in D_2O, respectively. Size exclusion chromatographic (SEC) analysis was carried out at 36 °C with a Waters 515 system, using a Waters 2410 differential refractometer as the detector. The eluant used was DMF containing 2.5 g/L of tetrabutylammonium bromide to eliminate polymer adsorption and peak tailing [45]. The columns used (Waters Styragel HR5E, Waters Styragel HR4E and μStyragel 500 Å) were calibrated using monodisperse polystyrene (PS) standards.

2.6. Co nanoparticle preparation and purification

All reactions were performed in a 50-mL three-neck round-bottom flask under nitrogen atmosphere. An example preparation involved first mixing in the flask 0.010 g of PEG-*b*-PAA containing 0.013 mmol of carboxyl groups and 0.0128 g (0.032 mmol) of TOPO in 9.55 mL of anhydrous 1,2-dichlorobenzene. The mixture was then heated to 185 °C and bubbled with N_2 for 5 min to remove moisture before 0.0445 g (0.130 mmol) of $Co_2(CO)_8$ in 0.45 mL of anhydrous 1,2-dichlorobenzene was injected rapidly. After 5 min of reaction the heating was stopped, by removing the reaction flask from the heating mantle.

In this example preparation, the concentrations of the carboxyl group ($[COOH]_0$), of TOPO ($[TOPO]_0$), and of Co(0) ($[Co]_0$) were 1.30, 3.2, and 26 mM, respectively, based on the final 1,2-dichlorobenzene solvent volume of 10.0 mL. Unless mentioned otherwise, the $Co_2(CO)_8$ decomposition time used in other runs was always 5 min.

Co nanoparticles were purified immediately after their preparation. This involved adding 25 mL of diethyl ether slowly into the reaction mixture under stirring, and then centrifugation at 1100 *g* for 5 min to settle the Co nanoparticles. Since TOPO and $Co_2(CO)_8$ were soluble and the excess PEG-*b*-PAA surfactant existed as micelles in the 1,2-dichlorobenzene/diethyl ether mixture, they remained in the supernatant and were removed by decantation. The black precipitate was re-dispersed into 5 mL of methylene chloride and separated as a precipitate by adding 10 mL of diethyl ether. After this procedure was repeated, the precipitate was vacuum-dried at room temperature to give 18.5 mg of sample. Th yield calculated from the ratio between the mass of the product and the total mass of the fed Co(0) and PEG-*b*-PAA was 73%.

2.7. Co nanocrystal characterization

The particles were sprayed on a carbon-coated copper grid before observation by transmission electron microscopy (TEM). TEM images were obtained using a Hitachi H-7000 instrument operated at 75 kV. Thermal gravimetric analyses (TGA) were carried out on a TA Q-500 instrument. A typical experiment involved raising the temperature from room temperature to 650 °C at 20 °C/min, and then holding the temperature at 650 °C for 20 min.

One Co particle sample with a TEM core diameter at 11.2 ± 3.3 nm was used for X-ray diffraction study. The sample was prepared by pressing 0.3345 g of the nanoparticles in a die under a hydraulic pressure of 1500 pounds per square inch to yield a disk. The X-ray diffraction experiment was performed on a Rigaku Ru 200b instrument using Cu Kα radiation at $\lambda = 0.15418$ nm.

Magnetic properties of three solid samples with TEM Co diameters of 10.9 ± 2.0, 13.3 ± 2.2, and 15.5 ± 2.9 nm were measured by a vibrating sample magnetometer (ADE Technologies). The corresponding PEG-*b*-PAA compositions of these samples were 59%, 47%, and 41%, respectively.

3. Results and discussion

3.1. Polymer synthesis and characterization

PEG-Br [46,47] and PEG-*b*-PtBA [48] were synthesized by using modified literature methods. The bromoisobutyryl terminal group of the resultant PEG-Br sample had a unique ^{1}H NMR peak at 1.94 pm, due to its six methyl protons. By comparing the integrated intensity of this peak with that of the ethylene proton peak of PEG at 3.5 ppm, we confirmed that the conversion of PEG-OH to PEG-Br was quantitative.

The resultant PEG-*b*-PtBA sample was characterized by SEC and ^{1}H NMR, with results shown in Table 1. The diblock copolymer had a SEC polydispersity index of 1.22, based on PS standards. The number of repeat unit ratio between PEG and PtBA was determined to be 15.1 from a comparison between the integrated intensities of the PEG peak at 3.5 ppm and a PtBA peak at 1.45 ppm. Using the manufacturer's number-average molar mass of $M_n = 5.0 \times 10^3$ g/mol for PEO, and the ^{1}H NMR value of $n/m = 15.1$, we obtained the number of repeat units of 113 and 7.5 for PEG and PtBA, respectively.

The hydrolysis of PtBA in dichloromethane/TFA has been practiced extensively in our group [49,50]. In this case, successful hydrolysis was confirmed by the disappearance of the tBA ^{1}H NMR peak at 1.35 ppm.

PEG-*b*-PAA with a relatively short PAA block was used because we suspected that many binding AA units per chain might lead to the irreversible binding of the chains to the growing Co nuclei and nanocrystals. As will be discussed later, this might lead to particles with a wide size distribution.

3.2. Results of Co nanoparticle preparations

Co nanoparticles were prepared from the rapid injection of $Co_2(CO)_8$ in 1,2-dichlorobenze into a reservoir of 1,2-dichlorobenze at 185 °C, in the presence of PEG-*b*-PAA and TOPO. This method is clean, since elemental cobalt is the only nonvolatile product of the reaction:

$$Co_2(CO)_8 \rightarrow 2\ Co + 8\ CO$$

For optimization of Co nanocrystal preparation, we examined how variations in the reaction temperature, the reaction time, and the concentrations of $Co_2(CO)_8$, PEG-*b*-PAA, and TOPO affected the sizes of the resultant Co nanocrystals. Table 2 gives the conditions for some of our preparations, and the size characteristics of the particles obtained from these preparations. The different batches were not listed in their batch number sequence but grouped to show a particular data variation trend or to facilitate data discussion.

The TEM diameter d and the spread of the diameter σ of each sample were obtained from analyzing TEM images of the resultant Co nanoparticles. Fig. 1 shows TEM images of samples from Batches 55 and 59, with their preparation recipes shown in Table 2. Since the samples were not stained before TEM observation, only the Co cores should be discernible here. Not all particles were strictly spherical, probably due to the fast rate of particle growth [7]. For the spherical particles the measurement of the diameter was straightforward. When the particles were not spherical, the d value was taken as the average length measured along the long and short axes of each particle, respectively. The d and σ values were obtained from the analysis of >140 Co nanoparticles for each sample.

Table 1
Characteristics of PEG-*b*-PtBA, the precursor to PEG-*b*-PAA.

SEC M_w/M_n	^{1}H NMR n/m	n	m
1.22	15.1	113	7.5

Table 2
Recipes and TEM sizes for different batches of Co nanoparticles.

Batch	$[Co]_0$/M	$[Co]_0/[COOH]_0$	$[COOH]_0/[TOPO]_0$	React. t (min)	TEM ($d \pm \sigma$) (nm)
Low-$[Co]_0$ Regime					
16	0.0065	2.0	1.0	5	7.4 ± 1.8
24	0.013	4.0	1.0	5	11.2 ± 3.3
$[Co]_0 = 0.026$ M					
28	0.026	20	0.40	5	17.4 ± 3.3
29	0.026	8.0	1.0	5	15.7 ± 2.7
27	0.026	4.0	2.0	5	12.7 ± 2.3
25	0.026	2.0	4.0	5	8.4 ± 1.9
26	0.026	1.3	6.0	5	7.3 ± 2.1
39	0.026	8.0	1.0	5	15.5 ± 2.9
33	0.026	20	0.40	5	17.7 ± 2.7
34	0.026	20	0.40	30	19.4 ± 2.9
32	0.026	20	0.40	60	18.8 ± 3.1
36	0.026	20	0.40	240	18.5 ± 3.0
38	0.026	8.0	∞	5	9.1 ± 4.0
High-$[Co]_0$ Regime					
54	0.080	8.0	3.0	5	10.8 ± 1.8
55	0.080	8.0	3.5	5	10.2 ± 1.8
58	0.15	15	3.4	5	17.0 ± 2.3
59	0.30	30	3.4	5	17.6 ± 2.5

Most of the Co nanoparticles in Fig. 1a and b were associated into chain-like structures. This should result from the magnetic dipole-dipole interactions between different Co nanoparticles [14,15,17,51]. Aside from the polymer-coated nanoparticles, we see in the TEM images prism-shaped thin discs, with some marked by arrows in Fig. 1b. We believe that these were PEG-*b*-PAA crystals that were formed from the crystallization of PEG at room temperature after solvent evaporation. We did not make an extra effort to remove them, because we thought some free PEG-*b*-PAA chains were always in equilibrium with the chains anchored on Co surfaces, and they would crystallize out when solvent was removed during TEM specimen preparation.

A close inspection of results of Table 2 revealed the following trends. First, the relative deviation σ/d of the Co nanoparticles ranged from ~14% to ~30%, which were substantially larger than those reported by Puntes et al [6,9,18]. when low-molar-mass surfactants were used as surfactants. Second, the σ/d value decreased as the initial Co(0) concentration, $2[Co_2(CO)_8]_0$ or $[Co]_0$, increased. Third, σ/d became very large, at 44%, when TOPO was not used. Fourth, d_{TEM} did not change significantly with reaction time t after 5 min. This is better seen in Fig. 2, which shows how d from TEM (d_{TEM}) changed for different batches of samples, such as Batches 33, 32, 34, and 36, which were prepared using different t. Fifth, d_{TEM} increased with increasing $[Co]_0/[COOH]_0$ at a given $[Co]_0$.

The increase in d_{TEM} with $[Co]_0/[COOH]_0$ is better seen in Fig. 3. To plot the data, we have artificially divided the data obtained in the presence of TOPO into three groups. Data of Group I were for samples prepared at $[Co]_0 = 0.026$ M, and were denoted by • in Fig. 3. Group II included data for samples prepared at $[Co]_0 \geq 0.080$ M, and their data were denoted by Δ in Fig. 3. Group III samples were those with $[Co]_0 \leq 0.013$ M, and their data were denoted by ○. For every group of samples, d_{TEM} increased with $[Co]_0/[COOH]_0$.

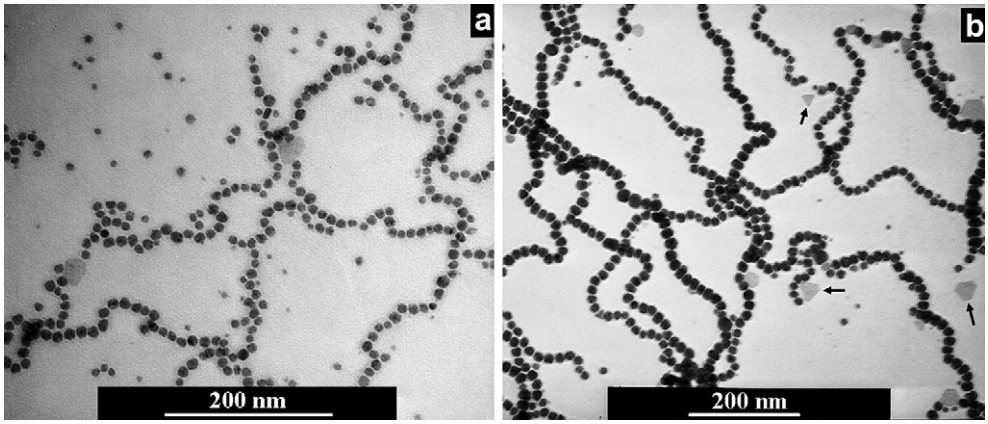

Fig. 1. TEM images of cobalt nanoparticle Batch 55 (a) and 59 (b).

3.3. Justification of experimental observations

According to classical theories [52–54], most inorganic crystals are obtained via two steps. In Step 1, very small embryos of the crystals are nucleated in a solvent. In Step 2, these nuclei grow to yield the crystals. The preparation of monodisperse nanocrystals is a nontrivial task, and requires the careful manipulation of the rates of nucleation and growth.

Classical theories stipulate that only embryos above a critical size would experience a decrease of their free energy with increasing size, and thus grow. Below this size, the embryos are more likely to decrease, than to increase, in size. These critical embryos, or nuclei, can form in a homogeneous solution, because the solution is super-saturated. Without consideration of the effect of the surfactant, LaMer showed that the rate of nuclei formation per unit volume was [52,55]:

$$\rho(t) = Dc^2 \frac{32\pi^2 a^3 \gamma}{3kT\ln(c/c_0)} \exp\left(-\frac{256\pi^3 a^6 \gamma^3}{27(kT)^3[\ln(c/c_0)]^2}\right) \quad (1)$$

Here c is the concentration of atoms, molecules or ions, that are generically called monomers of the crystal, present in the system at time t, c_0 is the solubility of a bulk crystal, a is the effective radius of a monomer unit in a crystal, D is the diffusion coefficient of the monomer, γ is the effective interfacial tension between a nuclei or crystal and its surrounding medium, and kT is the thermal energy. At a given temperature T, $\rho(t)$ evidently depends strongly on c. If $c < c_0$, $\rho(t)$ is negative, and the embryos are more likely to dissociate than to grow. A plot of Eq. (1) indicates that $\rho(t)$ starts to take off quickly from zero only at $c \approx 1.5c_0$. Thus, a critical nucleation concentration c_n with $c_n > c_0$ exists. Above c_n, nucleation occurs rapidly.

The growth of inorganic crystals has been traditionally assumed to be diffusion controlled [54,55]. Particles of different sizes grow at different rates for two reasons. First, more monomers are required to increase the radius of a spherical particle with a larger radius than a smaller radius r. Second, the solubility of spherical nanocrystals S_r increases with decreasing r following the Gibbs-Thomson equation [54]:

$$S_r = c_0 \exp\left(\frac{2\gamma a^3}{rkT}\right) \quad (2)$$

Assuming $\frac{2\gamma a^3}{rkT} << 1$, and a substantially larger diffusion layer thickness than the radius r of the Co nanocrystals, the diffusion-controlled growth rate for r is [54]:

$$\frac{dr}{dt} = \frac{K_D}{r}\left(\frac{1}{r^*} - \frac{1}{r}\right) \quad (3)$$

Here r^* is the critical nanocrystal radius at which the nanocrystal's solubility is equal to the bulk monomer concentration at time t or $S_{r^*} = c$, and K_D is:

$$K_D = \frac{2\gamma D a^6 c_0}{kT} \quad (4)$$

Equation (3) suggests that $dr/dt > 0$ only if $r > r^*$, or the particles grow with time only if their radius is larger than r^*.

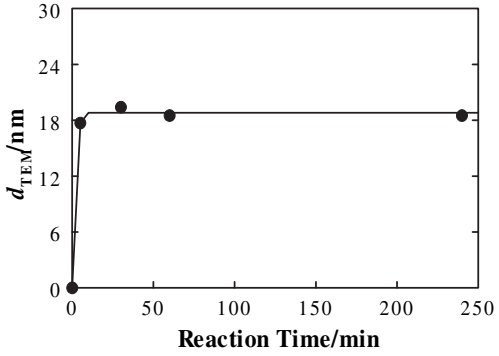

Fig. 2. Variation in d_{TEM} of the Co nanocrystals as a function of $Co_2(CO)_8$ decomposition time at 185 °C.

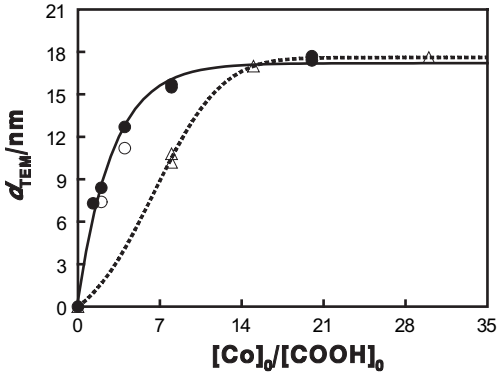

Fig. 3. Plot of d_{TEM} vs. $[Co]_0/[COOH]_0$ for samples prepared at $[Co]_0 < 0.026$ M (○), $[Co]_0 = 0.026$ M (●), and $[Co]_0 > 0.026$ M (Δ).

Equations (1) and (3) suggest that monomer concentration c and temperature T have a much more pronounced effect on $\rho(t)$ than on dr/dt. A conventional trick used to produce monodisperse nanocrystals is to use sufficiently high T and c to induce burst nucleation. Under these circumstances, the precursors decompose quickly, to produce a large amount of monomer, so that c_n is exceeded. The swift nucleation then reduces c down to c_n and nucleation essentially stops. It is between c_0 and c_n that growth takes place. By optimizing the temperature T and precursor concentration, one can, in principle, synchronize the rates of precursor decomposition and crystal growth, so as not to push c above c_n again. Thus, nucleation occurs only initially, and is followed by a growth process. The temporal resolution of the nucleation and growth processes ensures the production of monodisperse crystals [52–54].

Aside from the separation of the nucleation and growth processes, a preparation should be terminated during the size focusing stage, rather than during the size defocusing, or Oswald ripening stage [7,54–57]. A closer analysis of Eq. (3) reveals that smaller particles grow faster than the larger particles only if all of the particles have $r > 2r^*$. In the particle size focusing regime, the distribution of the particles narrows with time. As a reaction proceeds, the precursor and monomer concentration c decreases. This causes r^* to increase with time. By the time r^* becomes comparable with the mean particle size, the system enters the size defocusing regime, because the smaller particles have a smaller dr/dt than the larger ones, and can even have negative growth rates. Thus, monodisperse particles are prepared if the monomer concentration remains high throughout the preparation, before the particle size defocusing regime sets in. This is ensured again by the use of a relatively high precursor concentration, and also by the use of incomplete precursor conversion (not 100% conversion, but it can be very close to 100%, because the highest c that can be used is c_n, and c_n is normally very low).

In this study, the precursor used was $Co_2(CO)_8$ and the decomposition temperature of $Co_2(CO)_8$ was 52 °C [58]. Aside from using the sample preparation temperature of 185 °C, we also attempted the Co nanocrystal synthesis at 150 °C. Using the recipe for Batch 28 and $T = 150$ °C, we found that $Co_2(CO)_8$ did not undergo significant decomposition after 5 min, as judged from the retention of the dark blue color of $Co_2(CO)_8$. After 30 min at 150 °C, the reaction mixture turned black. The resultant Co nanocrystals had wide size distributions, however, with sizes ranging from several to ~50 nm. Smaller σ/d values were obtained at 185 °C, probably due to the better resolution of the nucleation and growth processes.

There are probably several reasons for the observed larger σ/d values when PEG-*b*-PAA, rather than oleic acid, was used as the surfactant for Co nanocrystal synthesis. First, we have probably not found the optimal conditions required for monodisperse particle preparation. Second, the stronger binding between Co and PEG-*b*-PAA, than between Co and oleic acid, should have reduced the Co monomer concentration in a given system. Our belief is that embryos, nuclei and growing nanocrystals were probably covered by PEG-*b*-PAA. The probability for a Co/PEG-*b*-PAA complex to add directly onto an embryo, a nucleus, or a nanocrystal should be much lower than a Co monomer, first due to the reduced diffusion of a complex relative to a Co atom, and then due to the greatly increased steric repulsion between a complex and the coronal PEG-*b*-PAA chains of a particle. As mentioned before, the use of low monomer concentrations c is not ideal, firstly due to the poor resolution of the nucleation and growth processes, and then because of the system's greater likelihood of entering the size defocusing regime. Third, there is a distribution in the number of AA units. These different binding strengths between the different surfactant molecules may render different growth rates to different particles, and thus lead to a broader Co particle distribution.

That the σ/d values decreased among the three groups of samples as $[Co_2(CO)_8]_0$ increased was in agreement with our prior discussion of the effect of increased $Co_2(CO)_8$ concentrations. The use of higher precursor, and thus monomer concentrations c, is more likely to improve the chances for a resolution of the nucleation and growth processes, and also to decrease the system's chances of entering the size defocusing regime.

The smaller σ/d values observed in the presence of TOPO has been traditionally accounted for by the dynamic binding nature of the TOPO ligand [6,10]. The dynamic binding of TOPO probably facilitates the swift deposition of Co monomers onto Co nanocrystals, and helps avoid the buildup of Co monomer concentrations above c_n, which would trigger further nucleation during the growth stage.

The production of larger particles at larger $[Co_2(CO)_8]_0/[COOH]_0$ values could be explained also by referring to Eqs. (1) and (3). As the surfactant content decreases, the extent of binding between PEG-*b*-PAA and Co monomers and nanocrystals decreases, and c may increase. The effective interfacial tension γ between Co and the solvent should also increase. An examination of the exponent of Eq. (1) suggests that the effect of an increase of γ may dominate over the effect of an increase of c, and that $\rho(t)$ decreases with increasing $[Co_2(CO)_8]_0/[COOH]_0$. The rate of growth should increase with increasing $[Co_2(CO)_8]_0/[COOH]_0$, according to Eqs. (3) and (4), because of an increase in K_D. A decreased number of nuclei formed should thus result in the formation of fewer nanocrystals, and the average size of the nanocrystals should increase.

3.4. Reaction yields

As mentioned before, carbonyl is volatile and should escape from the system after reaction. We determined gravimetrically the masses of Batches 28, 29, and 27. The yields were calculated as the ratios between the actual product mass and the theoretical maximal mass, which should be the sum of that of Co(0) in $Co_2(CO)_8$, and that of PEG-*b*-PAA used. Table 3 shows that the yields are substantially lower than 100%, because PEG-*b*-PAA that was not bound to the Co nanocrystals was mostly removed during sample purification. As $[Co_2(CO)_8]/[COOH]$ increased, d_{TEM} and the yield increased.

To determine the percentage of conversion from $[Co_2(CO)_8]$ to Co(0) nanocrystals, we determined the polymer weight fractions in the PEG-*b*-PAA/Co nanocrystals of these three samples using TGA. Interpretation of the TGA data required the use of certain assumptions. In Scenario 1, we assumed that the Co nanocrystals survived the heating from 100 to 425 °C intact. At the same time, we assumed that the PEG-*b*-PAA coating decomposed into volatile products, just like pure PEG-*b*-PAA, with only ~3% residual carbon. This gave us Co(0) conversions y_{Co} of ~120% for all of the three samples. This conversion, which exceeded 100%, prompted us to assume in Scenario 2 that Co reacted with the decomposing PAA chains, to yield CoO during the heating process. This yielded us y_{Co} values close to 100% (Table 3) as we had expected. Thus, we suspect that the Co nanoparticles did react during the thermal analysis to form CoO, a conclusion we had also reached for PAA-*b*-PS-coated Co nanocrystals [16].

Table 3
TGA analysis results and Co conversion yields for several batches of samples.

Batch	TEM $(d \pm \sigma)$/nm	Yield	Fractional weight loss between 100 and 425 °C	y_{Co}
28	17.4 ± 3.3	73%	26%	93%
29	15.7 ± 2.7	61%	38%	97%
27	12.7 ± 2.3	41%	57%	94%

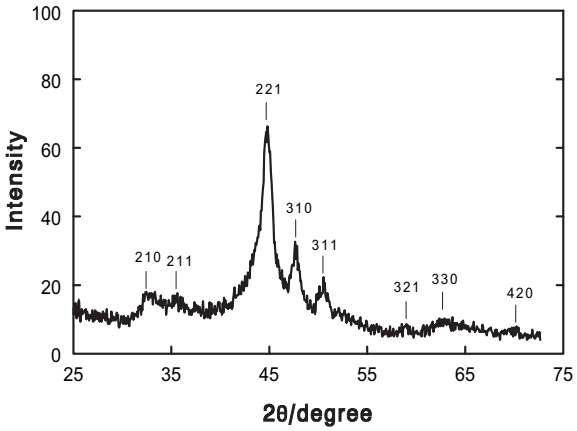

Fig. 4. X-ray diffraction data of a PEG-*b*-PAA/Co sample.

3.5. Crystal structure of Co

Illustrated in Fig. 4 are the X-ray diffraction data of batch sample 24 with a Co diameter of 11.2 ± 3.3 nm. The peak positions and intensity distribution of Fig. 4 bear exact resemblance to those reported for ε-Co nanoparticles [18,19]. Thus, the particles have the lattice structure of ε-Co nanoparticles.

The half-maximum width $\delta_{2\theta}$ for the (221) peak in Fig. 4 is 1.1°. Assuming that the small size of the cobalt particles was the dominant cause for peak broadening, we used the $\delta_{2\theta}$ value in the Scherrer equation [59]:

$$d_X = \frac{K\lambda}{\delta_{2\theta}\cos\theta} \tag{5}$$

to calculate the average diameter d_x of the particles. Here $\lambda = 0.15418$ nm. In order to assign the K value, we assumed that the particles were approximately spherical, and thus $K = 1.107$. This yielded a d_x value of 9.6 nm. This is in reasonable agreement with the TEM diameter of 11.2 ± 3.3 nm, considering that other peak broadening mechanisms may have also been at play. The reasonable agreement between the TEM and X-ray diameters suggests the single crystalline nature of the particles produced.

3.6. Core-shell structure of the Co nanocrystals

The particles should consist of a Co core surrounded by a monolayer of PEG-*b*-PAA, where PAA anchors onto the surfaces of the Co particles and PEG stretches out into the solvent phase. This PEG-*b*-PAA layer was seen sometimes by TEM when the carbon-coating on a TEM grid was thin. Fig. 5 shows such an image. A parallel pair of lines was drawn to bound the core and the shell of a particle, respectively. The shell layer is clearly visible for most of the particles in this image. Averaging over 100 particles, we obtained a mean thickness of 6.1 nm for the diblock layer, which is about 7 times smaller than the fully-stretched length of the PEG block.

3.7. Re-dispersion of the PEG-b-PAA/Co nanocrystals

Addition of the PEG-*b*-PAA/Co nanocrystal dispersions in 1,2-dichlorobenzene into excess diethyl ether induced precipitation of the nanocrystals. The addition of solvents such as DMF, dichloromethane, chloroform, ethyl acetate, and water after supernatant removal from the precipitate led to the quick redispersion of the nanocrystals. After drying the particles under vacuum, the nanocrystals turned into dense lumps, which were redispersed only slowly in the above solvents.

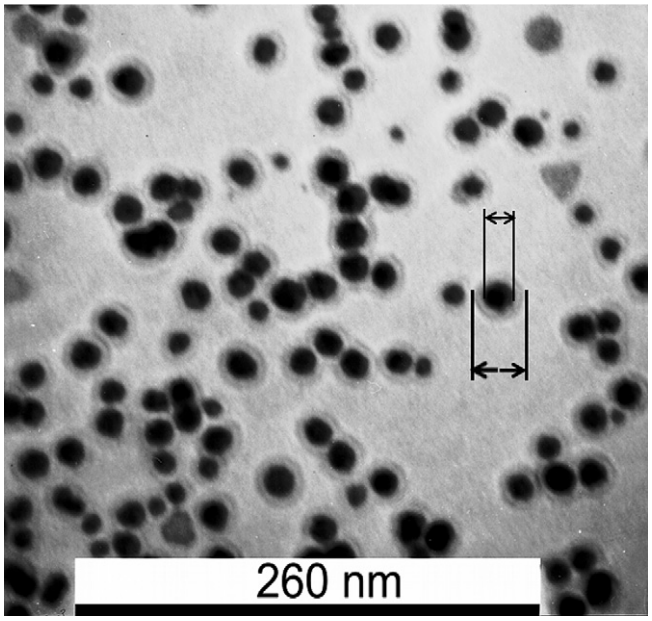

Fig. 5. TEM image showing the core-shell structure of PEG-*b*-PAA/Co nanocrystals obtained from Batch 39.

These dispersions in organic solvents such as dichloromethane in sealed bottles were chemically stable for months, as judged from the retention of the magnetic properties of Co. The colloidal stability of the particles depended on the particle size. For a sample with $d_{TEM} = 8.4 \pm 1.8$ nm, the particles settled from dichloromethane only after 2 weeks. On the other hand, batch 39 with $d_{TEM} = 15.5 \pm 2.9$ nm settled after approximately 3 days. For all samples with $d_{TEM} < \sim 18$ nm, the settled particles could be readily re-dispersed after agitation. The Co nanoparticles were highly dispersible in water as well. Unfortunately, the Co nanoparticles seemed to lose their magnetic properties over approximately 10 h, probably due to the oxidation of Co.

3.8. Magnetic properties

We have also obtained the magnetization curves, Fig. 6, for three samples. From the curves, we determined the saturation magnetization M_S, remanent magnetization M_R, and coercivity H_c for the samples and the results are given in Table 4. As d_{TEM} increased, the particles became progressively ferromagnetic, with M_R and H_c increasing. In all cases, the M_S values were high, approaching 161 emu/g for bulk Co [60]. A saturation magnetization lower than that of bulk materials is normal for nanoparticles. Typical reasons for this behaviour include the reaction or complexation of the surface atoms of magnetic nanoparticles with surfactant, which may create a layer with no magnetization [61]. With a significant fraction of surface atoms, any crystalline disorder within the surface layer may also lead to a significant decrease in nanoparticle saturation magnetization. The similarities between

Table 4
Magnetic properties of three batches of PEG-PAA/Co nanoparticles.

Batch	TEM ($d \pm \sigma$)/nm	Polymer weight fraction	M_S (emu/g)	M_R (emu/g)	H_c (kOe)
39	15.5 ± 2.9	41%	123	21.8	0.110
41	13.3 ± 2.2	47%	134	15.0	0.044
42	10.9 ± 2.0	59%	137	10.0	0.028

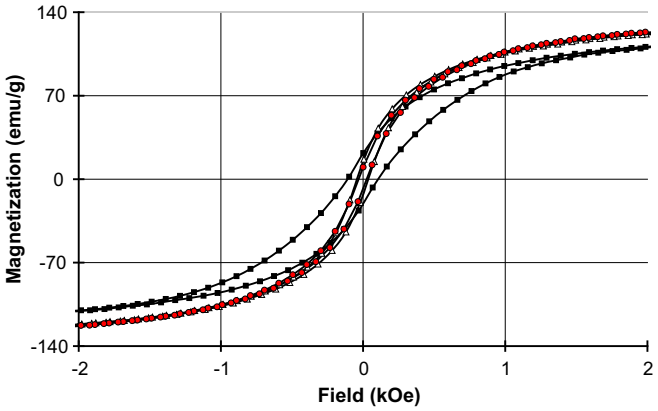

Fig. 6. Magnetization curves for Batch 39 (■), 41 (Δ), and 42 (●) PEG-PAA/Co nanoparticle samples.

the M_S values of our Co nanoparticles and those of bulk Co suggests the high purity of the Co crystals, and also a negligible surface deactivation effect.

4. Conclusions

A PEG-*b*-PAA diblock copolymer has been synthesized and characterized. This diblock copolymer, consisting of 113 EG units and ~7.5 AA units, worked well as the surfactant in the preparation of PEG-*b*-PAA/Co nanocrystals. These crystals were prepared via the thermal decomposition of $Co_2(CO)_8$ in the presence of the diblock copolymer surfactant PEG-*b*-PAA and co-surfactant TOPO. At 185 °C in 1,2-dichlorobenzene, the nanoparticles were formed within 5 min. The size of the particles increased, at a given initial $Co_2(CO)_8$ concentration, with $[Co_2(CO)_8]_0/[PEG\text{-}b\text{-}PAA]_0$, and could be reproducibly tuned between ~5 and ~20 nm. Particles with the lowest polydispersities were produced at the highest $[Co_2(CO)_8]_0$, and these results could be justified by classical crystal nucleation and growth theories. The lattice structure of the nanocrystals was determined by X-ray diffraction to be ε-Co, and the particles were dispersible in a wide range of solvents, including water, which solubilized PEG. Magnetic measurements revealed that the particles possessed saturation magnetization values very close to those of bulk Co, suggesting the high purity of the particles.

Acknowledgement

The EMK program of Materials and Manufacturing Ontario is gratefully acknowledged for financially sponsoring this research. We thank Mr. Matthias Haeussler and Professor Ben Zhong Tang of the University of Science and Technology of Hong Kong for assistance with obtaining the magnetization curves. Dr. Ian Wyman is thanked for proof-reading this manuscript.

References

[1] Kaplan LA, Pesce AJ. Clinical chemistry – theory, analysis, and correlation. St. Louise: CV Mosby Co.; 1989.
[2] Schnur JM. Science 1993;262:1131.
[3] Black CT, Murray CB, Sandstrom RL, Sun SH. Science 2000;290:1131.
[4] Weller D, Sun SH, Murray C, Folks L, Moser A. IEEE Trans Magnet 2001;37:2185.
[5] Thurn-Albrecht T, Schotter J, Kastle CA, Emley N, Shibauchi T, Krusin-Elbaum L, et al. Science 2000;290:2126.
[6] Puntes VF, Krishnan KM, Alivisatos AP. Science 2001;291:2115.
[7] Yin Y, Alivisatos AP. Nature 2005;437:664.
[8] Puntes VF, Zanchet D, Erdonmez CK, Alivisatos AP. J Am Chem Soc 2002;124:12874.
[9] Puntes VF, Krishnan K, Alivisatos AP. Top Catalys 2002;19:145.
[10] Murray CB, Sun SH, Gaschler W, Doyle H, Betley TA, Kagan CR. IBM J Res Dev 2001;45:47.
[11] Sun SH, Murray CB. J Appl Phys 1999;85:4325.
[12] Thomas JR. J Appl Phys 1966;37:2914.
[13] Hess PH, Parker PH. J Appl Polym Sci 1966;10:1915.
[14] Keng PY, Shim I, Korth BD, Douglas JF, Pyun J. Acs Nano 2007;1:279.
[15] Pyun J. Polymer Rev 2007;47:231.
[16] Liu GJ, Yan XH, Lu ZH, Curda SA, Lal J. Chem Mater 2005;17:4985.
[17] Zhou ZH, Liu GJ, Han DH. Acs Nano 2009;3:165.
[18] Puntes VF, Krishnan KM, Alivisatos P. Appl Phys Lett 2001;78:2187.
[19] Dinega DP, Bawendi MG. Angew Chem Int Ed 1999;38:1788.
[20] Tracy C, Gao J. Appl Phys Lett 2005;87.
[21] Pei QB, Yu G, Zhang C, Yang Y, Heeger AJ. Science 1995;269:1086.
[22] Scrosati B, Croce F, Panero S. J Power Sources 2001;100:93.
[23] Murata K, Izuchi S, Yoshihisa Y. Electrochim Acta 2000;45:1501.
[24] Platonova OA, Bronstein LM, Solodovnikov SP, Yanovskaya IM, Obolonkova ES, Valetsky PM, et al. Colloid Polym Sci 1997;275:426.
[25] Lin XM, Sorensen CM, Klabunde KJ, Hajipanayis GC. J Mater Res 1999;14:1542.
[26] Rutnakornpituk M, Thompson MS, Harris LA, Farmer KE, Esker AR, Riffle JS, et al. Polymer 2002;43:2337.
[27] Tadd EH, Bradley J, Tannenbaum R. Langmuir 2002;18:2378.
[28] Kastle G, Boyen HG, Weigl F, Lengl G, Herzog T, Ziemann P, et al. Adv Funct Mater 2003;13:853.
[29] Yan XH, Liu GJ, Haeussler M, Tang BZ. Chem Mater 2005;17:6053.
[30] Park IW, Yoon M, Kim YM, Kim Y, Kim JH, Kim S, et al. J Magn Magn Mater 2004;272–76:1413.
[31] Forster S, Antonietti M. Adv Mater 1998;10:195.
[32] Klingelhofer S, Heitz W, Greiner A, Oestreich S, Forster S, Antonietti M. J Am Chem Soc 1997;119:10116.
[33] Seregina MV, Bronstein LM, Platonova OA, Chernyshov DM, Valetsky PM, Hartmann J, et al. Chem Mater 1997;9:923.
[34] Mossmer S, Spatz JP, Moller M, Aberle T, Schmidt J, Burchard W. Macromolecules 2000;33:4791.
[35] Moffitt M, Vali H, Eisenberg A. Chem Mater 1998;10:1021.
[36] Li Z, Liu GJ. Langmuir 2003;19:10480.
[37] Underhill RS, Liu GJ. Chem Mater 2000;12:3633.
[38] Underhill RS, Liu GJ. Chem Mater 2000;12:2082.
[39] Horiuchi S, Fujita T, Hayakawa T, Nakao Y. Langmuir 2003;19:2963.
[40] Chan YNC, Schrock RR, Cohen RE. J Am Chem Soc 1992;114:7295.
[41] Kane RS, Cohen RE, Silbey R. Chem Mater 1999;11:90.
[42] Liu GJ, Ding JF, Hashimoto T, Kimishima K, Winnik FM, Nigam S. Chem Mater 1999;11:2233.
[43] Selvan ST, Hayakawa T, Nogami M, Moller M. J Phys Chem B 1999;103:7441.
[44] Yan XH, Liu GJ, Liu FT, Tang BZ, Peng H, Pakhomov AB, et al. Angew Chem Int Ed 2001;40:3593.
[45] Kim C, Morel MH, Sainte Beuve J, Guilbert S, Collet A, Bonfils F. J Chromatogr A 2008;1213:181.
[46] Wegrzyn JK, Stephan T, Lau R, Grubbs RB. J Polym Sci Part A Polym Chem 2005;43:2977.
[47] Hou SJ, Taton D, Saule M, Logan J, Chaikof EL, Gnanou Y. Polymer 2003;44:5067.
[48] Sun XY, Zhang HL, Huang XH, Wang XY, Zhou QF. Polymer 2005;46:5251.
[49] Li Z, Liu G, Law SJ, Sells T. Biomacromolecules 2002;3:984.
[50] Lu ZH, Liu GJ, Duncan S. Macromolecules 2004;37:174.
[51] Butter K, Bomans PHH, Frederik PM, Vroege GJ, Philipse AP. Nat Mater 2003;2:88.
[52] Lamer VK. Ind Eng Chem 1952;44:1270.
[53] Lamer VK, Dinegar RH. J Am Chem Soc 1950;72:4847.
[54] Sugimoto T. Adv Colloid Interface Sci 1987;28:65.
[55] Park J, Privman V, Matijevic E. J Phys Chem B 2001;105:11630.
[56] Peng XG, Wickham J, Alivisatos AP. J Am Chem Soc 1998;120:5343.
[57] Reiss HJ. Chem Phys 1951;19:482.
[58] Blums E, Cebers A, Maiorov MM. Magnetic fluid. New York: Walter de Cruyter; 1997.
[59] Klug HP, Alexander LE. X-ray diffraction procedures for polycrystalline and amorphous materials. New York: John Wiley & Sons; 1954.
[60] Weast RC, Lide DR, Astle MJ, Beyer WH. CRC handbook of chemistry and physics. 70 ed. Boca Raton: CRC Press; 1989.
[61] Burker NAD, Stover HDH, Dawson FP. Chem Mater 2002;14:4752.